s100A9

E-mail:

Abstract

Inflammation is one of the prominent pathological feature in Alzheimer's disease (AD). About the role of the neuroinflammation, there are some debated views such as driving forces, bystander, byproduct or neuroprotective response emerging in recent literature. S100A9 as one of the pro-inflammatory protein is abundant and over-expressed in the inflammation sites of AD, the role of S100A9

This study presents a potential role of pro-inflammatory protein S100A9 in the Aβ oligomerization process, which may contribute to the understanding of the etiology and pathogenesis of AD.

*To whom correspondence should be addressed

Introduction

Alzheimer's disease (AD) is characterized by amyloid-β (Aβ) plaques and neurofibrillary tangles. The deposition of the Aβ peptides and the accumulation of the tau protein filaments tangles are suggested to be directly associated with prominent neuroinflammations.[1–4] Moreover, the neuroinflammations are significantly correlated with the cognitive impairment.[5]

Aβ oligomers are believed to be the most toxic culprit in AD and the aggregation of Aβ peptides forming oligomers turns out to be an important pathological pathways.[6–8] Aβ oligomers accompany with deposits may provoke the activation of astro- and microglia, and initiate a series of chronic inflammation process in AD brains. Clinical studies reveals that anti-inflammation drugs can delay the early-onset and progression of AD, but merely weakly improve the cognitive impairment.[4,9] Meanwhile, the neuroprotective effect of inflammation has also been considered as an beneficial response in AD.[10–13]

Phagocytic S100 proteins belong to the EF-hand Ca^{2+}-binding protein family. They regulate a plethora extracellular and intracellular processes such as cell growth and differentiation, calcium homeostasis, inflammation response and etc.[14] S100A8 (myeloid-related protein, MR8), S100A9 (calgranulin B; MRP14) and S100A12, three inflammation-associated proteins in S100 family, are abundantly over-expressed and actively secreated by non-traditional Golgi-route pathway at the inflammation sites.[15] S100A8 and S100A9 tend to coexpress and exist as heterotetramer complex, which are highly stabilized and able to confer some indispensable functional roles.[16,17]

S100A9 can also express and function independently without forming hetero-dimer with S100A8. The enhanced expression of S100A9 is observed in AD brains. The knockdown of S100A9 gene shows a great improvement in the cognitive impairment in Tg2576 mice and a reduced amounts of Aβ.[18] The pro-inflammatory effect of S100A9 partially relies on its binding to other receptors like Toll-like receptors (TLRs).[19] The binding of calcium to S100A9 induces an exposed broad hydrophobic surface to interact with other proteins and further modulate the target, or reciprocally induce S100A9 its own or with S100A8 self-assembly into homo- or heterodimers or even high order oligomers.

Recent experimental study shows that the binding of S100A9 towards the Aβ peptide pro-

motes the formation of Aβ plaques, accordingly reduces the toxic Aβ oligomers and further plays a protective response in AD brains.[13]

In this article, we are going to perform replica exchange molecular dynamic (REMD) simulation to examine the interaction of S100A9 with Aβ peptide. Aβ_{12-24} is took as the representative of the full-length Aβ peptide, which has been reported to be able to assist explore fundamental aspects of the thermodynamics and kinetics of Aβ oligomerization process.[20–22] Furthermore, Aβ_{12-24} contains one of the central hydrophobic region, whose inter-chain interaction, hydrogen bond match pattern and dimerization process in the presence of S100A9 will shed some light in understanding the effect of S100A9 on the full-length Aβ oligomerization process.

Methods and simulation setup

The S100A9 dimeric structure consists of two tightly packed EF-hand motifs, which composed of helix-loop-helix region, connected by a linker (also dubbed as "hinge") region. The homodimeric structure of S100A9 was took from Protein Data Bank (PDB) ID: 1IRJ[16] with 4 calcium and 2 extended $_{12}$VHHQKLVFFAEDV$_{24}$ Aβ peptides were represented by AMBER99SB force field and solvated in a cubic box of dimensions 92.574 Å $\times$ 71.590 Å $\times$ 105.702 Å. 42 Na^+ and 44 Cl^- were added to the 22235 water molecules to reach the concentration of 0.1 mol/L.

The peptides were capped by N-terminal acetyl group and C-terminal amide group. The protonation state of HIS, LYS, ARG and ASP are listed in Support Material Table S1. S100A9 was restrained in the center of the cubic box with a constant force of $2000 kJmol^{-1}nm^{-2}$ applied on the homo-dimer and $1000 kJmol^{-1}nm^{-2}$ on the calcium. The two peptides were random placed around the S100A9, and 108 different conformations were took as starting structures to reduce the bias to the least and accelerate the REMD convergence.

All bonds were constrained using the linear constraint solver (LINCS)[23] algorithm with a 2 ps accurate leap-frog molecular dynamics integration time step. The Van der Waals cutoff was set to 1.2 nm. 0.9 nm range cut-off were used for electrostatic interactions. The S100A9,

calcium, two Aβ peptides and solvent were separately coupled to an external heat bath with a relaxation time of 0.1 ps. The temperatures of the 108 replicas in our REMD simulations are listed in Support Material and approximately 30% averaged acceptance ratio with exchange between neighboring replicas tried every 2 ps has achieved. The simulation cumulative time is 22.14 μs with total 22140000 structures were generated.

The REMD simulations and analysis were using GROMACS package.[24–26] PyMOL[27] and VMD[28] were used to visualize the structure. Additional analysis and visualization were assisted by plotmtv, MATLAB, originPro and some in-house scripts.

Results

Characterization of the Aβ dimer conformations

Dimer distribution regards the temperature

The self-assembly of Aβ_{12-24} forming into dimer was observed in our study. The last 10 ns were took to characterize the dimer distribution and structure diversity. The maximum density of dimers, is found between 315 K and 342 K with an average amount proportion of 20.7% in the last 10 ns. Whereas single monomers are dominant at high temperatures (> 402 K). Meanwhile the number of residues adopted β-structure decreased with the increase of the temperature.

Parallel and antiparallel β-sheet patterns

The parallel and anti-parallel β-sheet pattern were examined using all sampled configurations at 315 K. 36900 first bridge pattern are identified, which are consisted of 180 parallel and 36720 anti-parallel patterns. Two paired residue numbers are denoted by i and j. $i-j$ indicates the parallel patterns, while $i+j$ indicates the anti-parallel patterns. For the parallel β-sheets (see Figure 1(a)), the highly populated patterns include: (1) $i-j=\pm3$ (35.5%); (2) $i-j=\pm5$ (18.9%); (3) $i-j=\pm7$ (15.6%) and (4) $i-j=\pm9$ (13.3%). For the anti-parallel β-sheets (see Figure 1(b)), the highly populated patterns include: (1) $i+j=39$ (30.12%); (2) $i+j=35$

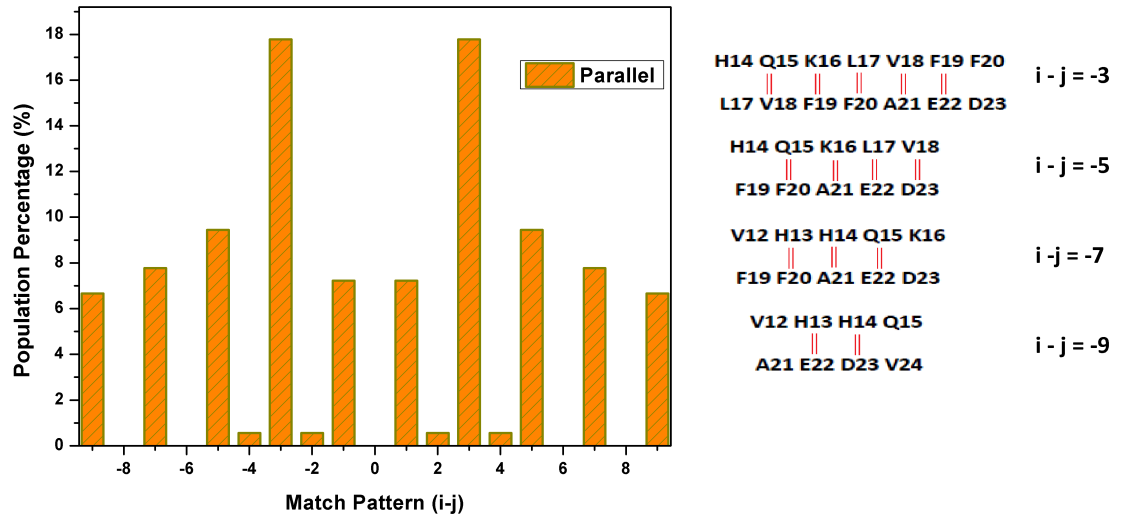

(a)

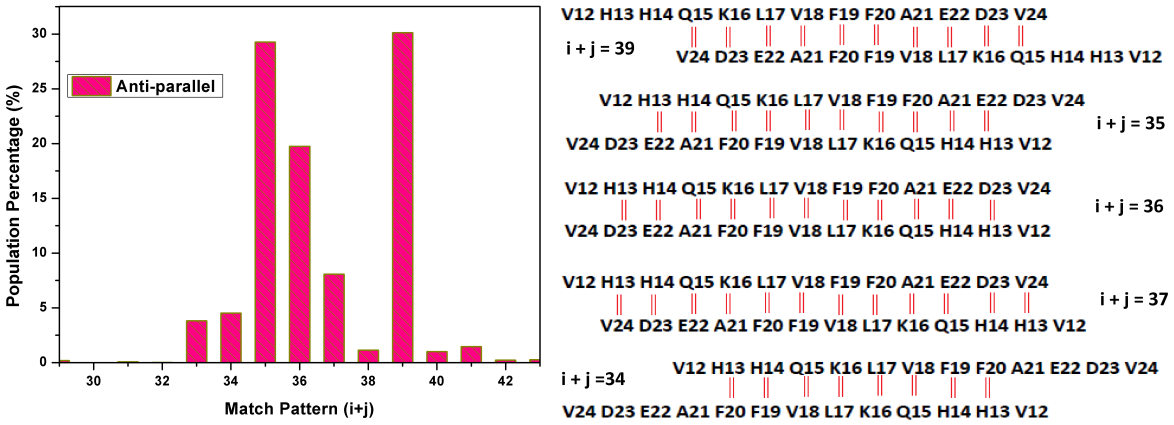

(b)

Figure 1: Population of various matching patterns for the parallel (a) and antiparallel (b) alignments. The representative of highly populated parallel and anti-parallel Aβ_{12-24} dimerization pattern are given with the red vertical lines denote hydrogen bond.

(29.28%); (3) $i+j=36$ (19.74%); (4) $i+j=37$ (8.06%); (5) $i+j=34$ (4.5%) and (6) $i+j=33$ (3.8%).

The diversity of the populated β-sheet registries were also reported on same[29,30] or other Aβ fragments such as Aβ_{16-22}, Aβ_{16-35}, Aβ_{10-35}[20,31,32] and even mutated Aβ_{29-42} fragments.[33] Comparison to the study of the same fragment (namely Aβ_{12-24}) dimer formation at different pH levels,[30] some new patterns emerged in our studies, which may be related to many factors, such as the different pH, different replicas and also the presence of the S100A9.

Aβ_{12-24} secondary structure propensity

The last 50 ns ensemble averaged secondary structure propensity of each residue were calculated at 315 K (see Figure 2). The secondary structure propensity was categorized into four classes: bend and turn; coil; β-structure (β bridge and β-sheet) and helix (α-helix and 3-helix). The helical conformation is very low for each residues. The same result was also observed in the similar study of Aβ_{12-24} under different pH values.[30] From residue HIS-14 to GLU-22 all shows the same preference of adopting coil, then bend & turn and β-structure. Furthermore, the β-structure of each residue decreased with the increase of the temperature.

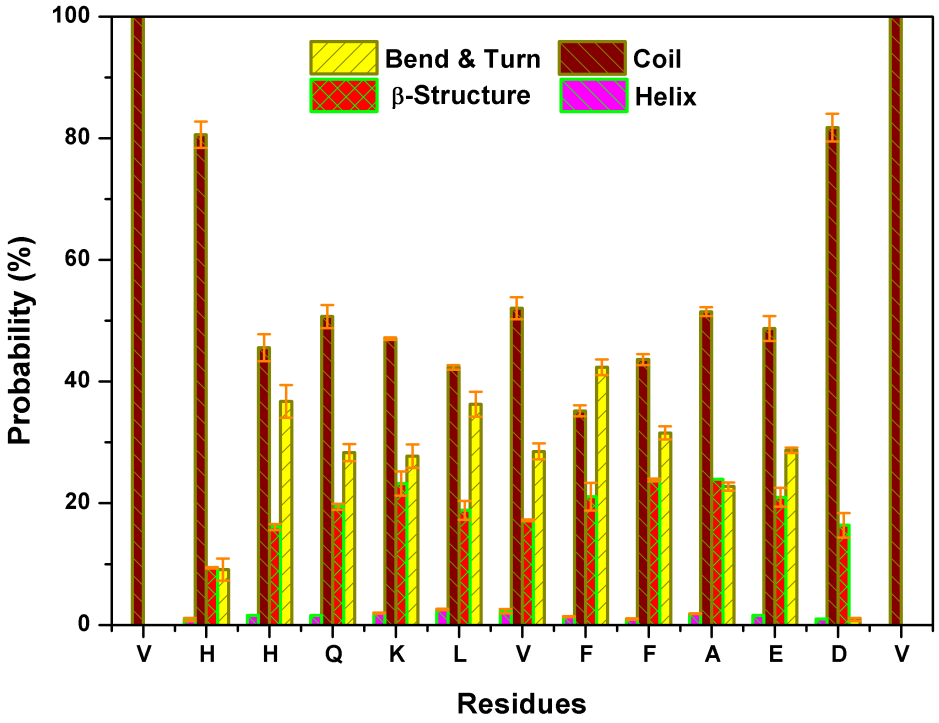

Figure 2: Secondary structure propensity of each residues at $T = 315$ K in the last 50 ns.

Free energy landscape

Dihedral angle principal component analysis (dPCA) method,[34] based on the transformation of the peptide dihedral angles, is conducted to construct the free energy landscape. Several free energy minima accompanied with the characteristic secondary structures were shown in Figure 3.

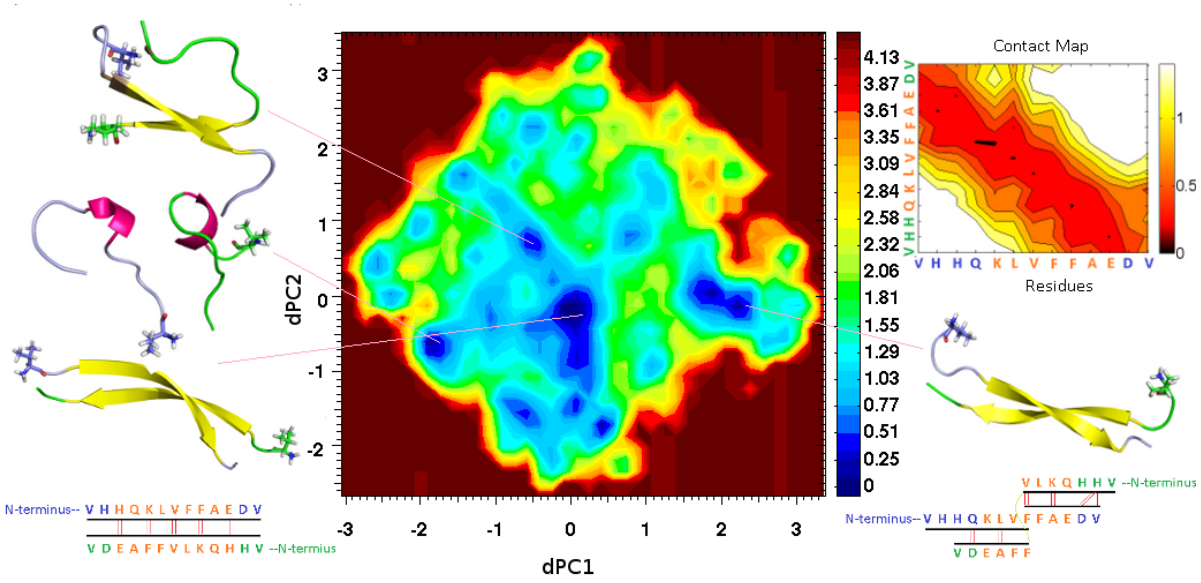

Figure 3: Free energy landscape in the last 50 ns as a function of the first two dihedral principal component dPC1 and dPC2 was plotted. Four representative structures at local minima were shown in cartoon (β-sheet: Yellow; 3-10-Helix: Purple; Coil: Lightblue for peptide A, green for peptide B). The N-terminus of peptide A and B were showed in stick and colored by element (N: blue; H: grey; O: red). The hydrogen bond forming information from two popular anti-parallel-β-sheet dominant structures were illustrated at the bottom (Blue residues indicate it from peptide A, green from peptide B, the orange residues indicate they are sitting on β structure.). One contact map is plotted to show the detailed contact information. The figures were generated by Plotmtv, PyMol[27] and Matlab.

Characterization of the interaction between Aβ and S100A9

Kinetics of amyloid oligomerization

It's been reported that amyloid oligomerization is mainly induced by Aβ rather than by S100A9.[13] To better examine the role of S100A9 in the dimerization process, we calculated the number of hydrogen bonds between Aβ peptides and S100A9, and the number of hydrogen bonds and contact numbers between two peptides. We found that the number of hydrogen bonds forming between Aβ peptides and S100A9 has a high positive correlation with the number of contacts between the two peptides (with a Pearson correlation coefficient of 0.88). While the number of hydrogen bonds forming between the two peptides shows a negative correlation with the number of contacts (with a Pearson correlation coefficient of -0.22). We concludes that S100A9 plays a major role in the induction of the oligomerization process. Furthermore we examined

the relationship between the Aβ-sheet length (the number of residues adopted β-structure) and the minimum distance between Aβ and S100A9. We found that the longest β-sheet is pretty near the S100A9 (See Support Material Figure.)

Potential of mean force of dimerization

The ensemble of extensive configurations obtained in our REMD simulation providing an alternative channel to calculate the potential of mean force (PMF) during Aβ dimerization.

To examine the potential of mean force in the presence of S100A9, a one-dimensional grid was constructed with respect to the distance between the center of mass of the two central hydrophobic cluster (CHC) (namely from 17-21) heavy atom and minimum distance between CHCs and S100A9 to count the number of sampled conformations in each bin, denoted as N_i. The potential of mean force V_{pmf} is:

$$V_{pmf} = -k_B T log(N_i/N_{max}). \tag{1}$$

Here k_B is the Boltzmann constant, T is the absolute temperature and N_{max} is the maximum number of sampled conformations counted in each bin.

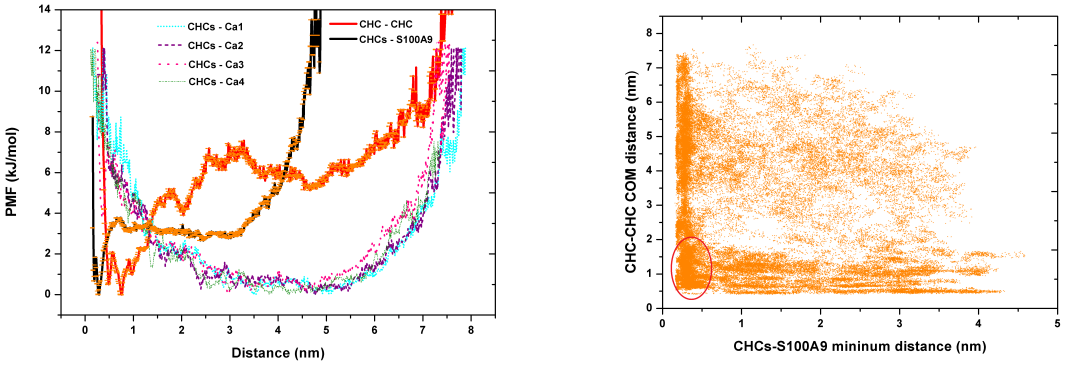

(a) (b)

Figure 4: (a) Potential of mean force (in kJ/mol) at 315 K. The four Calcium atoms are labeled as Ca1-Ca4. The error bars are shown in orange dash for CHC-CHC and CHC-S100a9. (b) The density distribution of CHC-CHC COM distance with respect to the minimal distance towards S100A9 at 315 K. x-label indicates the minimum distance between CHCs and S100A9, y-label represents the COM distance between the two CHC. The red circle indicated the densest distribution area.

From Figure 4(a), we can see that the basin of the CHC-CHC PMF curve is located in the range of inter-chain distance $5-10\mathring{A}$ with global minimum around 7.6 Å, which corresponds to the Aβ dimerization distance. We can see that Aβ posses the lowest free energy as dimer. To examine the influence of the S100A9 in the Aβ dimerization, the PMF based on the minimum distance between CHCs and S100A9 (see Figure 4(a)) and the density distribution of CHC-CHC COM distance with respect to the minimal distance towards S100A9 (see Figure 4(b)) were plotted. The PMF curve indicates that the basin exists in the range of $2.5-3.3\ \mathring{A}$ with global minimum at 2.9 Å, which corresponds to the densest Aβ dimer distribution (indicated by red circle line in Figure 4(b)). Furthermore it implies that S100A9 may facilitate Aβ dimerization.

Calcium-dependent and -independent interactions

The larger Ca^{2+} ions, unlike Mg^{2+} ions which interact strongly with six water molecules forming $[Mg(H_2O)_6]^{2+}$, do not bind water molecules very tightly, which gives the readiness to be displaced by other anions. The calcium mostly posses seven or eight co ordinations.[35]

Secondary structure transition in S100A9/Aβ peptide

the S100A9/Aβ interaction does not result in any change in S100A9 secondary structures.[13]

dimer conformations have higher free energies compared to their corresponding monomeric states) Our results suggest that Ab oligomerization is not accompanied by the formation of thermodynamically stable planar b-strand dimers

to explore the diversity of conformations adopted by the dimer

Characterization of the interaction between Aβ and S100A9

Aβ_{12-24} and S100A9 linker

Acknowledgement

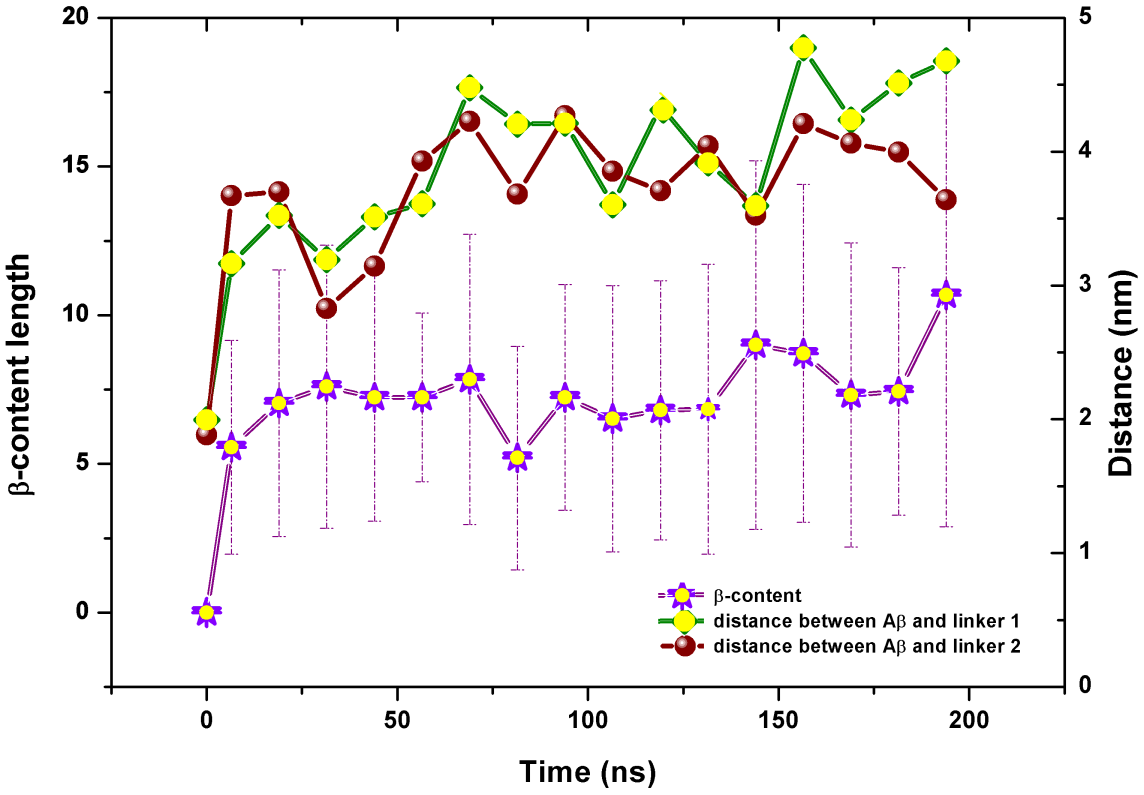

Figure 5: The number of Aβ_{12-24} residues adopt β-content structure (β-sheet and β-bridges) at 315 K and its COM distance away from the center of S100a9 linker 1 and linker 2, respectively. The number of β-content and the COM distance were calculated at every 500 ps interval within the total simulation time of 205 ns, and averaged at every 12.5 ns.

References

(1) Tuppoa, E. E.; Arias, H. R. *The International Journal of Biochemistry and Cell Biology* **2005**, *37*, 289–305.

(2) Akiyama, H. et al. *Neurobiology of Aging* **2000**, *21*, 383–421.

(3) Tan, Z. S.; Seshadri, S. *Alzheimer's research & therapy* **2010**, *2*, 6.

(4) Heneka, M. T.; O'Banion, M. K. *Journal of Neuroimmunology* **2007**, *184*, 69–91.

(5) Holmes, C.; Cunningham, C.; Zotova, E.; Woolford, J.; Dean, C.; Kerr, S.; Culliford, D.; Perry, V. H. *Neurology* **2009**, *73*, 768–774.

(6) Zhao, L. N.; Long, H.; Mu, Y.; Chew, L. Y. *Int. J. Mol. Sci.* **2012**, *13*, 7303–7327.

(7) Zhao, L. N.; Chiu, S.-W.; Benoit, J.; Chew, L. Y.; Mu, Y. *J. Phys. Chem. B* **2011**, *115*, 12247–12256.

(8) Shankar, G. M.; Li, S. M.; Mehta, T. H.; Garcia-Munoz, A.; Shepardson, N. E.; Smith, I.; Brett, F. M.; Farrell, M. A.; Rowan, M. J.; Lemere, C. A.; Regan, C. M.; Walsh, D. M.; Sabatini, B. L.; Selkoe, D. J. *Nature Medicine* **2008**, *14*, 837–842.

(9) Cameron, B.; Landreth, G. E. *Neurobiology of Disease* **2010**, *37*, 503–509.

(10) Wyss-Coray, T. *Nature Medicine* **2006**, *12*, 1005–1015.

(11) Salminen, A.; Ojala, J.; Kauppinen, A.; Kaarniranta, K.; Suuronen, T. *Progress in Neurobiology* **2009**, *87*, 181–194.

(12) Tripathy, D.; Thirumangalakudi, L.; Grammas, P. *Neurobiology of Aging* **2010**, *31*, 8–16.

(13) Zhang, C.; Liu, Y.; Gilthorpe, J.; van der Maarel, J. R. C. *PLoS One* **2012**, *7*, e32953.

(14) Heizmann, G. F. C. W.; Schäfer, B. W. *Frontiers in Bioscience* **2002**, *7*, 1356–1368.

(15) Rammes, A.; Roth, J.; Goebeler, M.; Klempt, M.; Hartmann, M.; Sorg, C. *J. Biol. Chem.* **1997**, *272*, 9496–9502.

(16) Itou, H.; Yao, M.; Fujita, I.; Watanabe, N.; Suzuki, M.; Nishihira, J.; Tanaka, I. *J. Mol. Biol.* **2002**, *316*, 265–276.

(17) Vogl, T.; Gharibyan, A. L.; Morozova-Roche, L. A. *Int. J. Mol. Sci.* **2012**, *13*, 2893–2917.

(18) Chang, K.-A.; Kim, H. J.; Suh, Y.-H. **2012**, *10*, 27–29.

(19) Foell, D.; Wittkowski, H.; Vogl, T.; Roth, J. *Journal of Leukocyte Biology* **2007**, *81*, 28–37.

(20) Nguyen, P. H.; Li, M. S.; Derreumaux, P. *Phys. Chem. Chem. Phys.* **2011**, *13*, 9778–9788.

(21) Melquiond, A.; Dong, X.; Mousseau, N.; Derreumaux, P. *Curr. Alzheimer Res.* **2008**, *5*, 244–250.

(22) Ma, B.; Nussinov, R. *Curr. Opin. Chem. Biol.* **2006**, *10*, 445–452.

(23) Hess, B.; Bekker, H.; Berendsen, H. J. C.; Fraaije, J. G. E. M. *J. Comput. Chem.* **1997**, *113*, 1463–1472.

(24) Berendsen, H. J. C.; van der Spoel, D.; van Drunen, R. *Comput. Phys. Comm.* **1995**, *91*, 43–56.

(25) Lindahl, E.; Hess, B.; van der Spoel, D. *J. Mol. Model* **2001**, *7*, 306–317.

(26) Spoel, D. V. D.; Lindahl, E.; Hess, B.; Groenhof, G.; Mark, A. E.; Berendsen, H. J. C. *J. Comput. Chem.* **2005**, *26*, 1701–1718.

(27) DeLano, W. L. The PyMOL Molecular Graphics System, Version 1.4, Schrödinger, LLC. 2011.

(28) Humphrey, W.; Dalke, A.; Schulten, K. *J. Mol. Graphics* **1996**, *14*, 33–38.

(29) Abe, H.; Kawasaki, K.; Nakanishi, H. *J. Biochem.* **2002**, *132*, 863–874.

(30) Xu, W.; ; Zhang, C.; Derreumaux, P.; Graslund, A.; Morozova-Roche, L.; Mu, Y. *PLoS One* **2011**, *6*, e24329.

(31) Ma, B.; Nussinov, R. *Proc. Natl. Acad. Sci. U.S.A.* **2002**, *99*, 14126–14131.

(32) Balbach, J. J.; Ishii, Y.; Antzutkin, O. N.; Leapman, R. D.; Rizzo, N. W.; Dyda, F.; Reed, J.; Tycko, R. *Biochemistry* **2000**, *39*, 13748–13759.

(33) Lu, Y.; Wei, G.; Derreumaux, P. *J. Phys. Chem. B* **2011**, *115*, 1282–1288.

(34) Mu, Y.; Nguyen, P. H.; Stock, G. *Proteins: Struct. Funct. Bioinf.* **2005**, *58*, 45–52.

(35) Permyakov, E.; Kretsinger, R. H. *Calcium Binding Proteins (Wiley Series in Protein and Peptide Science)*; Wiley; 1 edition, 2011.